

# Geotechnical Tomography: The Effects of Diffraction

**REFERENCE:** Potts, B. D. and Santamarina, C., "Geotechnical Tomography: The Effects of Diffraction," *Geotechnical Testing Journal*, GTJODJ, Vol. 16, No. 4, December 1993, pp. 510–517.

**ABSTRACT:** Tomographic imaging is the inversion of a field parameter using boundary observations. Current techniques make different simplifying hypotheses. In geotechnical tomography the straight ray assumption is most common. Problems arise when the wavelength is of the same order of magnitude as the size of the inclusion. In this case, the physics of diffraction creates significant effects behind the anomaly, limiting the applicability of ray assumptions. This experimental study addresses the effect of diffraction and its potential consequences on inversion problems. The investigation is conducted using inclusion size to wavelength ratios between 1 and 10, with objects of various relative velocity and impedance. Travel times, power density, and signal duration are analyzed. Results demonstrate the healing effects of diffraction, frequency and impedance-dependent backscatter, and energy focusing. Hand-picked and cross-correlation-based travel times are compared. It is shown that both low- and high-velocity inclusions may become undetectable at some distance behind the object, that there is little effect of frequency on travel time but significant effect on power spectral density, and that high-velocity inclusions may be detected as low-velocity inclusions when travel time data are used.

**KEYWORDS:** geophysical methods, tomography, inversion, diffraction, crosshole testing

Tomographic imaging is the inversion of a field parameter using boundary measurements. In the context of geotechnical applications, waves are emitted into an unknown region and received at locations on the periphery. Inversion attempts to reconstruct the medium that would act as the proper transfer function between the input signal and the output.

Most work conducted so far has centered on the inversion of travel times to reconstruct the velocity field (Tallin and Santamarina 1990). Ray assumptions are generally made in this type of solution. Wielandt (1987) used numerical simulation to demonstrate the consequences of diffraction on measured travel times. He concluded that diffraction limits the applicability of ray-based inversions.

This paper presents a brief discussion of ray assumptions and diffraction from the point of view of geotechnical tomography. Wielandt's study and findings are summarized. Then, an experimental investigation of the effects of diffraction as a function of wave length and inclusion type is discussed.

<sup>1</sup>Undergraduate student and associate professor, respectively, Department of Civil Engineering, University of Waterloo, Waterloo, Ontario N2L-3G1, Canada.

## Ray Assumption and Diffraction

The interaction of waves with inclusions depends primarily on the size of the inclusion,  $D$ , relative to the wave length,  $\lambda$ . The ray assumption generally applies when  $D/\lambda \gg 1$ .

### Ray Assumption

Travel time is the integral of the reciprocal of the velocity,  $v$ , over the traveled path from a source,  $a$ , to a receiver,  $b$

$$t = \int_a^b \frac{1}{v} \cdot ds$$

Since ray path is a function of the velocity field, it is not possible to know the ray path in advance, the integral cannot be evaluated, and the problem is nonlinear. The problem may be linearized assuming that the straight path is the path of shortest travel time; this is known as the "straight ray assumption." However, first arrivals correspond to travel paths that minimize time, not distance. For example, in the case of a homogeneous medium with a high-velocity inclusion, nonstraight rays that travel through a high-velocity anomaly could arrive at a receiving point before the straight ray.

The straight ray assumption dominated developments in geotechnical tomography during the 1980s, as an extension of X-ray tomographic imaging in medical applications. From optics, the straight ray approximation applies if (Dines and Lytle 1979): (1) the travel length  $L \gg \lambda/2\pi$ , (2) the slow variation of the refraction index is such that straight ray is a good description, and (3) the wavelength is much smaller than the skin depth, i.e., distance at which the signal attenuates to  $1/e$ . Condition 2 constrains the relative impedance of the inclusion with respect to the background. Dines and Lytle (1979) concluded on the basis of limited data that velocity contrasts lower than 16 to 30% could be successfully inverted using linear ray tomography. If these conditions do not apply, yet  $D \gg \lambda$ , ray bending due to refraction can be taken into consideration in iterative algorithms. However, the problem is nonlinear, and difficulties with local minima, convergence, and uniqueness increase.

### Travel Time

An additional difficulty in travel-time-based inversions is the precision required in the measurement of travel times and the effect of errors in the back calculation of travel paths. Assuming homogeneous isotropic media, an error,  $\Delta t$ , in the measurement

of the travel time,  $t_0$ , could be interpreted as a deviation,  $\delta$ , at the midpoint of the straight path,  $L_0$ . A simple analysis based on the Pythagorean relation shows that (Santamarina and Cesare 1992)

$$\left(\frac{\delta}{L_0}\right) = \frac{1}{2} \sqrt{\left(\frac{\Delta t}{t_0} + 1\right)^2 - 1} \quad (1)$$

Therefore, a 1% error in the measurement of  $t_0$  results in an uncertainty,  $\delta$ , in the length of the travel path of 7%  $L_0$ . Therefore, measurement errors may override the effect of small low-velocity inclusions and affect the planning of experimental studies, e.g., separation of sources and receivers.

### Diffraction

When the size of inclusions,  $D$ , is in the same order of magnitude as the wavelength,  $\lambda$ , the ray approximation does not apply, and propagation must be considered from the point of view of the wave front and scattered energy. In this case, the full signature is used. Inversion algorithms in diffraction tomography have been developed (Pan and Kak 1983; King, Witten, and Reed 1989; Devaney 1982).

### Fermat's Ellipse

It follows from diffraction-based analyses that the position of diffractors that affect the wave arrival at the source is related to the wave length,  $\lambda$ . Indeed, waves scattered from diffractors within an ellipse, so that the travel distance,  $L^* \leq L + \lambda/4$  (the "first Fresnel zone"), will arrive approximately in phase with the direct wave that traveled the straight path,  $L$  (Nolet 1987). This observation parallels the previous discussion on the insensitivity of travel time to travel path in the context of ray assumptions.

### Simulation Studies

#### Huygens Simulation

Diffraction problems can be studied by replacing an existing wave front by Huygen wavelets in order to determine the position of the next front. A computer program with graphical output was written to simulate this process. The program generates wave fronts for first arrivals, but does not take amplitude and thus energy or attenuation into consideration.

A 10 by 10-m cross section was assumed in a homogeneous, isotropic medium, with velocity  $v_{\text{medium}} = 400$  m/s. A circular inclusion of diameter  $d = 3$  m was centered 5 m below the surface and 4 m from the left borehole. Two cases were simulated: (a) low velocity inclusion  $v_{\text{inc}} = 70$  m/s, and (b) high-velocity inclusion  $v_{\text{inc}} = 550$  m/s. The large contrasts enhance the differences in wave front with respect to circular fronts for the medium with no inclusion.

Results are presented in Fig. 1 with wave fronts at 2.5-ms increments for a source located in the left borehole at 5-m depth. First arrivals behind the low-velocity inclusion (Fig. 1a) are all diffracted waves and do not carry information about how low the velocity of the inclusion is; this occurs whenever some limiting value of the geometry and velocity contrast is reached. Hence, imaging with diffracted first arrival travel times and straight rays would not be appropriate in this case. On the other hand, the

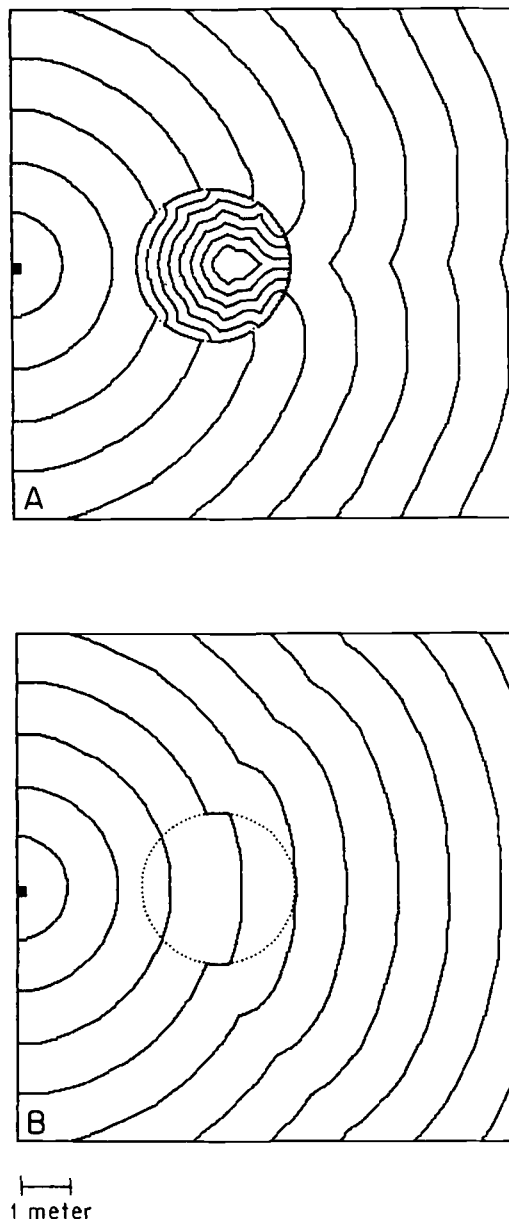


FIG. 1—Huygens simulation for a homogeneous, isotropic medium,  $v_{\text{med}} = 400$  m/s, with circular inclusion: (A) low-velocity inclusion,  $v_{\text{low}} = 70$  m/s; (B) high-velocity inclusion,  $v_{\text{high}} = 550$  m/s. Wave front interval = 2.5 ms.

front of first arrivals after the high-velocity inclusion (Fig. 1b) is clearly affected by the inclusion.

That high-velocity inclusions have enlarged projections on the detection plane is also shown in Fig. 1b. Furthermore, when the velocity of the anomaly is significantly larger than the medium, the excited inclusion appears as a weak source. Conversely, Fig. 1a indicates that when first arrivals are used for inversion, low-velocity inclusions have a reduced projection on the plane of the receivers.

A similar conclusion would be reached if  $D/\lambda \gg 1$  and ray theory applies: rays bend around low-velocity anomalies or in the direction of high-velocity anomalies; hence, images reconstructed assuming straight rays will be larger than the real high-velocity inclusion and smaller than the actual size of low-velocity inclusions.

### Wielandt's Study

Wielandt (1987) studied the effects of diffraction in reference to geophysical investigations of deep geological formations. He selected the case of a spherical inclusion in a homogeneous space, for which a full analytical solution is available, and solved it for the simpler case of acoustic waves, i.e., no shear waves.

The numerical simulation involved the generation of a plane wave and its detection at different points in a grid past the anomaly. The following parameters were used:

- wave velocity in the medium,  $v_{\text{medium}} = 8 \text{ km/s}$
- wave velocity in the inclusion,  $0.9 \cdot v_{\text{medium}} \leq v_{\text{incl}} \leq 1.1 \cdot v_{\text{medium}}$
- anomaly diameter,  $D = 100 \text{ km}$
- dominant frequencies: 1.5 and 5 Hz

The corresponding wavelengths,  $\lambda$ , are 5.33 and 1.6 km, respectively, yielding diameter to wavelength ratios,  $D/\lambda = 18.75$  and 62.5. The density of the inclusion was the same as that of the medium; therefore, the impedance mismatch is small, thus reducing backscatter. Wielandt's conclusions are (Wielandt 1987):

1. *High-velocity anomaly*: At a distance of  $4 \cdot D$  and off-centered from the axis of symmetry, the arrivals of different diffracted waves merge and the characteristics of the inclusion bear little consequence on the wave front. At about  $20 \cdot D$  behind the anomaly, the transmitted wave cannot be distinguished from the incident wave and the anomaly becomes invisible.

2. *Low-velocity anomaly*: Diffracted waves are strong enough at a distance of two inclusion diameters to be mistaken for the transmitted wave. While a minor delay remains, it is independent of the magnitude of the velocity anomaly. Amplitude of the diffracted signals is controlled by the frequency content, yet travel times are only slightly sensitive to changes in frequency.

Wielandt (1987) also showed that the straight ray assumption biases imaging and results in larger images of high-velocity inclusions and smaller images of low-velocity inclusions. These conclusions are in agreement with observations made in the previous section (Fig. 1).

### Experimental Study

#### Purpose

Geotechnical investigations often involve detection of small anomalies. However, the characteristic frequency of most sources used in soils seldom reaches the kHz range. For common ranges of velocity,  $D/\lambda$  ratios lower than those simulated by Wielandt (1987) take place. Therefore, an experimental study was designed to assess the effect of diffraction phenomena at lower  $D/\lambda$  ratios and under more realistic conditions including noise and spherical rather than planar incident wave front.

#### Methodology

Similar to Wielandt's simulation, this study was performed with acoustic waves; air was chosen as the medium. The signal was emitted by a speaker connected to a continuous signal generator through an off-on-off gate circuit. Three main frequencies were selected to be compatible with the other dimensions; these frequencies were 2000, 5000, and 8150 Hz ( $\lambda = 0.172$ , 0.069, and 0.042 m).

Signals were detected at four microphones and sampled with a digital oscilloscope at 500 kHz per channel without additional

filters or amplification. The frequency response of the microphones is flat in the 50 to 3000-Hz range and peaks at about 5000 Hz. Microphones were calibrated, and the response was normalized with respect to a common unit used for comparison. Their directional response was measured and shown to be negligible for orientations up to  $\pm 45^\circ$ . The gate circuit and the characteristics of the speaker and microphones created spurious harmonics affecting the received signals. Stored signals were analyzed using a commercial signal-processing package (DADisp).

The geometry of the experiment delayed echoes from boundaries to arrive significantly later than the main incident wave. Measurements were run in the room without inclusion to gather control data. Three inclusions were selected: (a) a steel pipe with significant impedance mismatch, (b) a helium balloon to emulate a high-velocity inclusion, and (c) a balloon filled with carbon dioxide to simulate a low-velocity inclusion. Dimensions of inclusions and test geometry are summarized in Fig. 2.

#### Typical Data

The three inclusions were tested at each of the three different frequencies, recording the signals in each of the four channels in every case. Typical results for the case of the helium inclusion at 8150 Hz, and for the steel pipe at 2000 Hz are shown in Figs. 3 and 4. The first column shows the time series recorded at the four receivers, the second column presents the power spectral density, and the third one shows the cross correlation of each signal with the record from the first channel. Vertical scales have been modified for presentation as data span several orders of magnitude. The scaling factor is noted in each window.

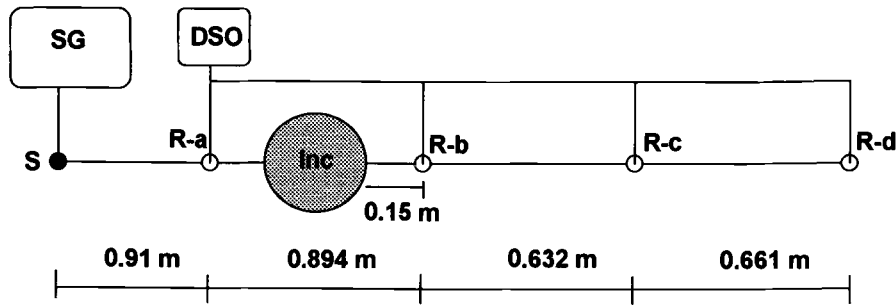
Signals are compared through three main parameters: travel time, signal duration, and power spectral density. Values are tabulated in Tables 1 and 2 and plotted in Figs. 5 and 6.

#### Travel Time

Two methods are used to determine travel times. First, travel times are picked manually from printed time series; second, travel times are obtained from cross correlation. Results are presented in Table 1. For comparison, travel times are calculated for ray paths of minimum travel time: shortest path around the pipe and the CO<sub>2</sub> balloon, and straight ray through the He inclusion. Standard values for the speed of sound were corrected for temperature and pressure resulting in  $v_{\text{air}} = 343.8 \text{ m/s}$ ,  $v_{\text{He}} = 1039 \text{ m/s}$ ,  $v_{\text{CO}_2} = 267 \text{ m/s}$  (measured balloon pressures are less than 3% atmosphere). Computed times are also shown in Table 1.

In the case of the steel pipe, manually picked first arrivals are significantly earlier than calculated minima (around the pipe through air) and cross correlation. The time difference is about 0.3 ms in all channels and at all frequencies. A possible explanation is that fast Raleigh waves travel along the shell of the pipe, leaking energy that arrives earlier at the receivers. These early signals carry little energy and are not recognized by the process of cross correlation.

In the case of the He inclusion, manually picked travel times are very similar to travel times computed assuming a straight ray through the balloon. Differences are in the same order as measurement errors, and no correlation with frequency is apparent. The cross correlation function shows several secondary peaks with similar amplitude to the largest peak, particularly for the receiver immediately behind the inclusion. In most cases, travel times based on cross correlation showed a positive delay (even though the impedance mismatch is small). Should cross corre-



**Notes:**

- SG      Signal Generator
- S        Speaker Source
- DSO     Digital Storage Oscilloscope (500 kHz)
- R        Microphone Receiver

**Inclusions:**

- He      D= 0.20 m       $v_{inc} = 1039 \text{ m/s}$        $Z_r = 0.50$
- CO<sub>2</sub>    D= 0.19 m       $v_{inc} = 267 \text{ m/s}$        $Z_r = 1.42$
- Steel    D= 0.33 m      thick= 7 mm

**Selected Frequencies:**

- 2000 Hz     $\lambda = .172 \text{ m}$        $D/\lambda = 1.1-1.9$
- 5000 Hz     $\lambda = .069 \text{ m}$        $D/\lambda = 2.8-4.8$
- 8150 Hz     $\lambda = .042 \text{ m}$        $D/\lambda = 4.5-7.9$

FIG. 2—Experimental setup (all inclusions and frequencies).

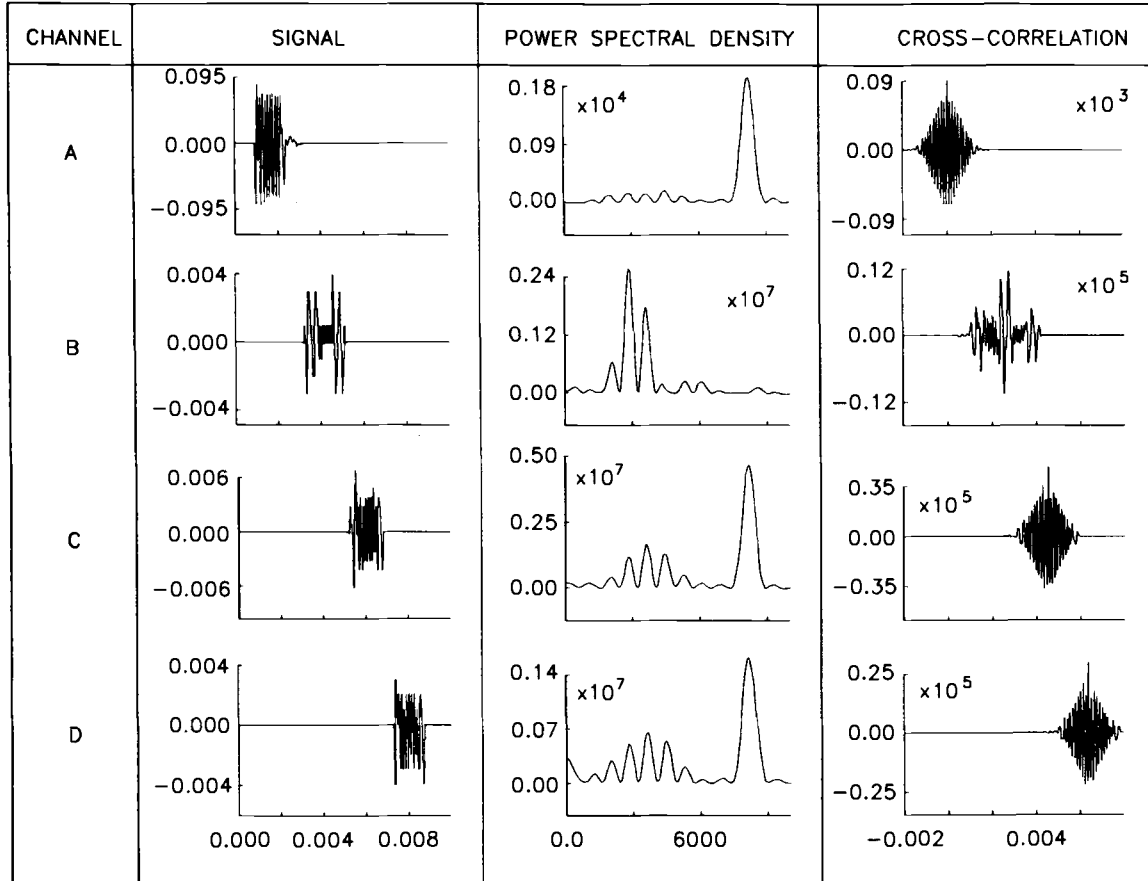


FIG. 3—High-velocity helium inclusion: signals recorded at different receivers ( $v_{inc} = 1039 \text{ m/s}$ ,  $D = 0.20 \text{ m}$ , selected frequency: 8150 Hz,  $I = 0.042 \text{ m}$ ).

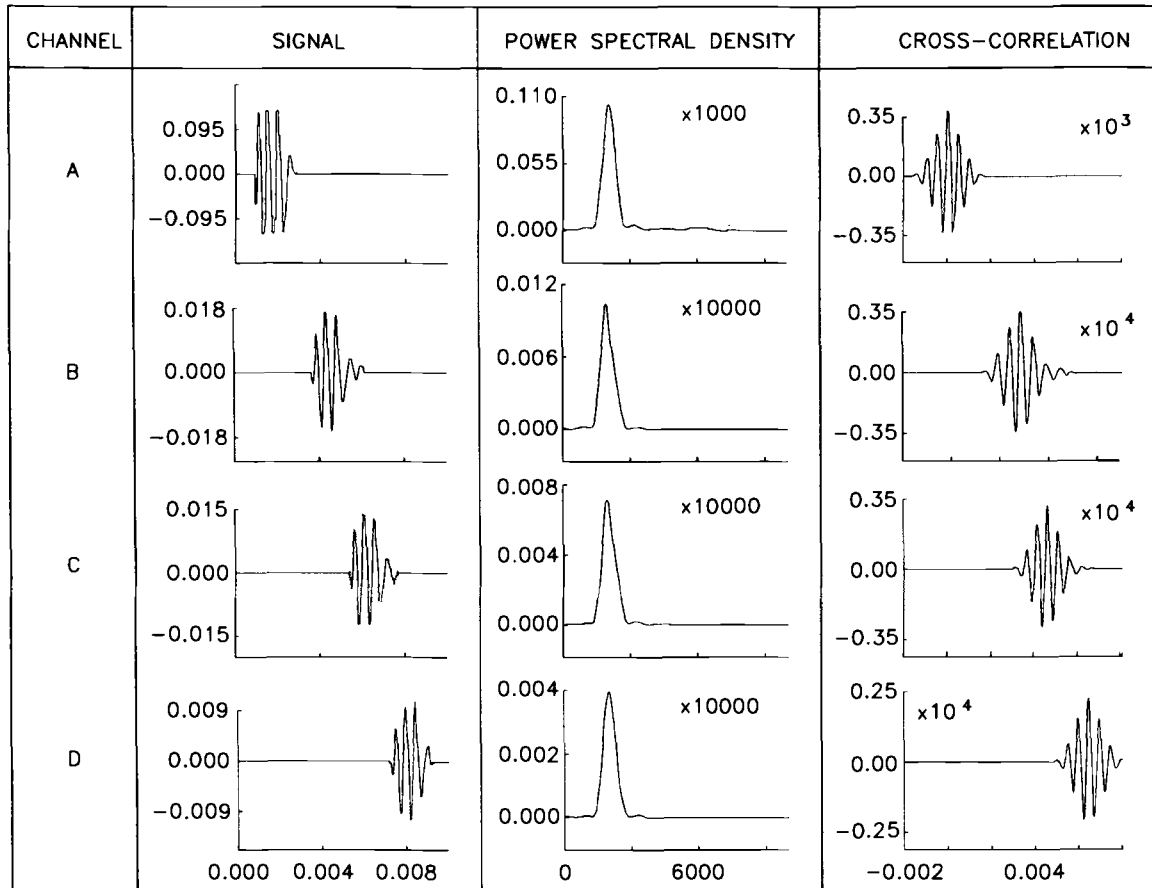


FIG. 4—Steel pipe inclusion: signals recorded at different receivers ( $D = 0.33$  m, selected frequency: 2000 Hz,  $I = 0.172$  m).

TABLE 1—Travel times.

Inclusion	Frequency, Hz	Observed, ms	Cross Correlation	Calculated, ms
None	All	2.57 ± 0.03	2.60 ± 0.0	2.60
		4.44 ± 0.03	4.44 ± 0.0	4.44
		6.33 ± 0.01	6.36 ± 0.0	6.36
Steel pipe	2000	2.59	2.83	2.80
		4.29	4.56	4.55
		6.04	6.46	6.46
Steel pipe	5000	2.58	2.80	2.80
		4.25	4.55	4.55
		6.02	6.44	6.46
Steel pipe	8150	2.56	2.85	2.80
		4.34	4.53	4.55
		6.19	6.42	6.46
Helium inclusion	2000	2.25	2.77 (2.31)	2.20
		3.99	4.49	4.04
		5.83	6.40	5.97
Helium inclusion	5000	2.25	2.35 (2.57)	2.20
		4.04	4.48	4.04
		5.93	6.38	5.97
Helium inclusion	8150	2.20	2.71 (2.36)	2.20
		4.04	4.47	4.04
		6.02	6.37	5.97
Carbon dioxide inclusion	2000	2.66	2.68	2.65
		4.43	4.45	4.45
		6.40	6.40	6.37
Carbon dioxide inclusion	5000	2.75	2.72	2.65
		4.56	4.48	4.45
		6.51	6.42	6.37
Carbon dioxide inclusion	8150	2.67	2.74	2.65
		4.43	4.44	4.45
		6.35	6.39	6.37

TABLE 2—Normalized signal duration.

Inclusion	Frequency, Hz	A	B	C	D
None	2000	1.00	1.00	1.00	1.00
None	5000	1.00	1.03	1.00	1.01
None	8150	1.00	1.01	1.00	1.01
Average		1.00	1.02	1.00	1.01
Steel pipe	2000	1.00	1.29	1.10	1.00
Steel pipe	5000	1.00	1.12	1.05	1.02
Steel pipe	8150	1.00	1.13	1.07	1.03
Average		1.00	1.18	1.07	1.02
Helium inclusion	2000	1.00	1.18	1.18	1.14
Helium inclusion	5000	1.00	1.30	1.19	1.13
Helium inclusion	8150	1.00	1.29	1.19	1.03
Average		1.00	1.26	1.19	1.10
Carbon dioxide inclusion	2000	1.00	1.00	1.00	0.97
Carbon dioxide inclusion	5000	1.00	1.08	1.08	1.00
Carbon dioxide inclusion	8150	1.00	1.16	1.08	1.00
Average		1.00	1.08	1.05	0.99

The duration of the signal increases immediately after the inclusion, indicating the arrival of signals from multiple paths. However, signal duration further behind the inclusion declines towards the original value. This is the result of path differences becoming relatively less significant and low-energy wave fronts fading away. The effect of the helium inclusion is more pronounced, reaching further into the field behind the inclusion.

Power Spectral Density

The power spectral density was determined for every signal. Stored signals were clipped before arrivals to reduce noise effects and after arrivals to cancel room echoes. Clipped signals were corrected for d-c offset and tail-packed with 0-values to increase frequency resolution. Power densities determined for Channels B, C, and D were normalized with respect to that of Channel A (before the inclusion) at the preselected characteristic frequency of the test. Results are plotted in Fig. 6. The inverse square law is shown for reference; control measurements in air without inclusion plot on this line. The normalized power spectral densities are plotted in logarithmic scale to highlight trends in the far field. Note that limitations in measurement and processing of low-energy signals are also magnified in this plot: in a linear scale, all trends clearly approach the no-inclusion case.

The higher the characteristic frequency of the signal, the higher the backscatter. For example, in the case of the steel pipe and 8150-Hz signals detected in the channels behind the inclusion, B, C, and D have very little energy, and the lower frequency harmonics present in the original signal prevail (see also Fig. 3). The increase in energy from Channel B to C is the result of diffraction. Similar trends are observed for the He inclusion and the steel pipe for the 8150-Hz characteristic frequency as well as the 5000-Hz signal. Backscatter is less significant for the 2000-Hz frequency signal with either inclusion ( $D/\lambda = 1.9$  and  $1.2$ ).

The CO<sub>2</sub> inclusion, on the other hand, acts as a convergent lens with low-impedance mismatch. The result is the focusing of energy in the near field behind the inclusion as manifested by the high-energy content in Channel B at all frequencies, in particular at 2000 and 5000 Hz, where the power density exceeds

lation results be used in standard imaging algorithms, a low-velocity anomaly would be obtained.

In the case of the CO<sub>2</sub> inclusion, small positive delays are observed in manually picked and cross-correlation-based travel times. The delay is most significant in the first sensor behind the inclusion (Channel B); in this case, the travel time is similar to the value estimated for the straight ray through the balloon. There are no significant differences between travel times obtained by cross correlation and manually picked values.

Signal Duration

The duration of the signal was measured from the printed time series. Results presented in Table 2 are normalized with respect to the signal duration determined from the first microphone (Channel A, in front of the inclusion—Fig. 2). Figure 5 presents average normalized duration of the signal versus the position of the receivers normalized with respect to the size of the inclusion.

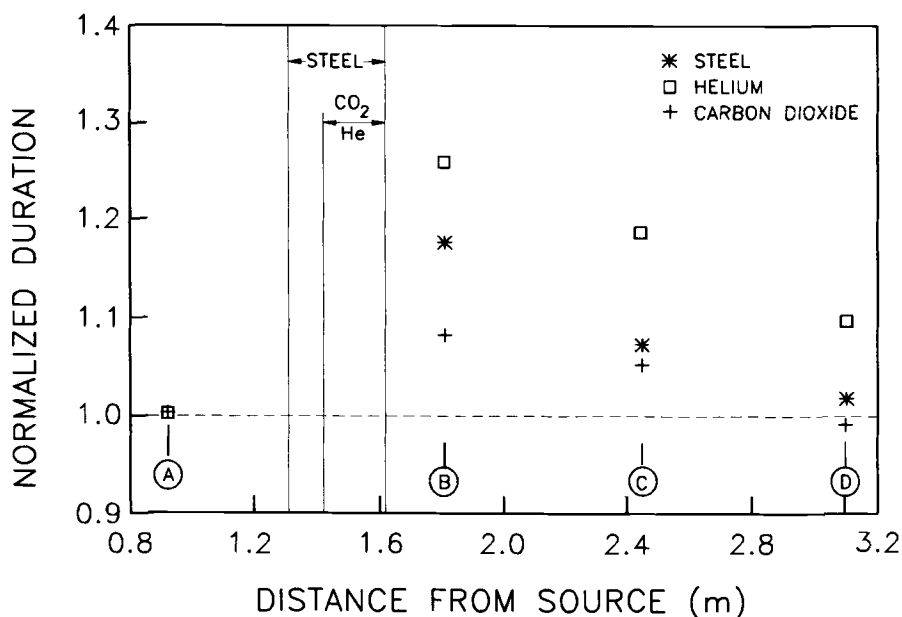


FIG. 5—Normalized signal duration as a function of distance—average values for the three selected frequencies (data for steel, helium, and carbon dioxide inclusions).

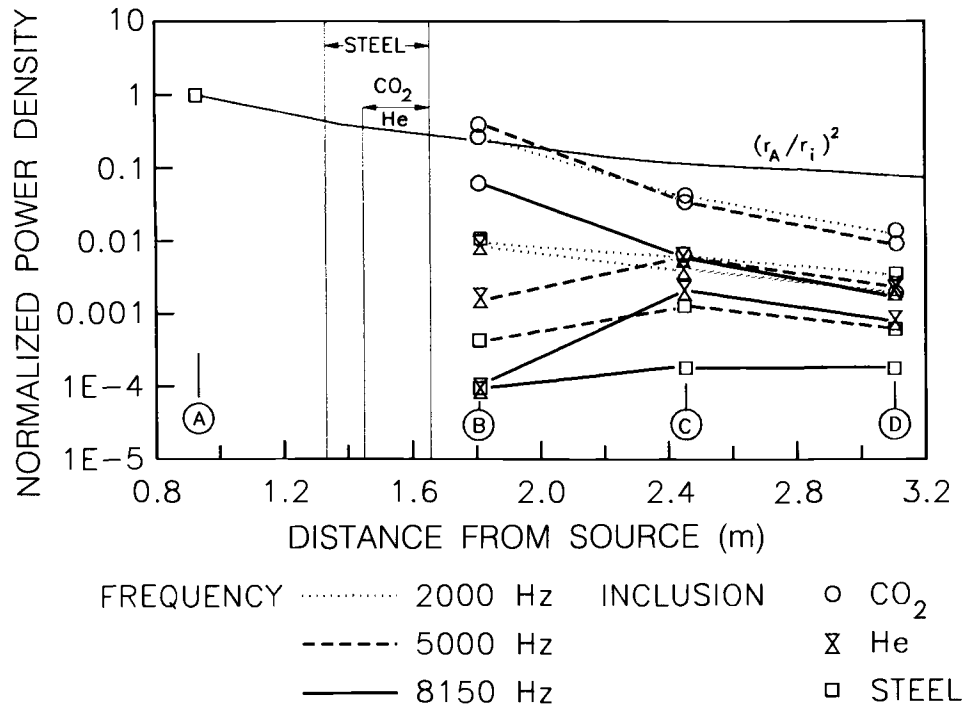


FIG. 6—Normalized power density as a function of distance and frequency (data for steel, helium, and carbon dioxide inclusions).

the control value for the medium without inclusion. Energy enhancement is affected by the frequency of the wave, the geometry of the anomaly, its relative impedance and refractive index. This phenomenon has been observed at all scales, from microseismicity in mines to earthquakes. It adds difficulty to the inversion of attenuation data and to the interpretation of resulting images.

### Conclusions

The effect of diffraction on received signals was evaluated. Huygen-based simulations, numerical analyses (from Wielandt 1987), and experimental measurements were presented. Results have significant relevance to the generation and interpretation of tomographic images.

Experimental observations can be explained by the combined effects of multiple paths, relative impedance and backscatter, diffraction, and energy enhancement. These observations, within the context of the tested parameters and geometry, are as follows:

1. Travel time and signal duration are little affected by the frequency of the wave. The effect of frequency is more significant on the ratio of power densities.

2. Our experimental results are in general agreement with results from numerical models conducted by Wielandt (1987). Together, they span a ratio of inclusion size to wave length from  $D/\lambda \approx 1$  to  $D/\lambda \approx 60$ . For higher ratios the effect of diffraction diminishes and ray models face less difficulties.

3. Signal duration, travel time, and power spectral density approach the no-inclusion condition away from any anomaly; this is called "diffraction healing" of wave fronts. Within the range of variables tested in this study, low-velocity inclusions are difficult to detect with any signal parameter at low  $D/\lambda$  when receivers are 4 to 6 diameters away from it. High-velocity inclu-

sions may be detected to longer distances (in the order of 10 inclusion diameters).

4. The combined effects of diffraction and impedance contrast limit the applicability of ray-based inversion algorithms. The higher the relative impedance of the inclusion, the lower the energy transmitted through, hence the lower the direct wave energy that will reach the receivers. Indeed, high-velocity anomalies with high-impedance contrast can appear as low-velocity inclusions when travel times are used in inversion algorithms.

5. Paths of minimum travel time may carry a small percentage of the incident energy, and first arrivals may be lost or not detected in the record. Travel time detection algorithms (e.g., selection of a first arrival by any arbitrary threshold or by using cross correlation) are biased by paths of high-energy content.

6. The straight ray assumption will produce smaller images of low-velocity inclusions, and larger images of high-velocity anomalies. This effect occurs through refraction as well as diffraction.

7. Energy enhancement is determined by the characteristics of the wave, the anomaly, and the medium. This phenomenon affects the inversion and interpretation of attenuation data.

### Acknowledgments

This research was supported by the Natural Sciences and Engineering Research Council of Canada. The authors are thankful to reviewers for their useful comments and suggestions.

### References

Devaney, A. J., 1982. "A Filtered Back Propagation Algorithm for Diffraction Tomography," *Ultrasonic Imaging*, No. 4, pp. 336-350.

- Dines, K. and Lytle, J., 1979, Computerized Geophysical Tomography, *Proceedings of IEEE*, Vol. 67, pp. 1065–1073.
- King, W. C., Witten, A. J., and Reed, G. D., 1989, "Detection and Imaging of Buried Wastes Using Seismic Wave Propagation," *ASCE Journal of Environmental Engineering*, Vol. 112, No. 3, pp. 527–540.
- Nolet, G., 1987, "Seismic Wave Propagation and Seismic Tomography," *Seismic Tomography*, G. D. Nolet, Ed., Reidel Publishing Co., Boston, pp. 1–23.
- Pan, S. X. and Kak, A. C., 1983, "A Computational Study of Reconstruction Algorithms for Diffraction Tomography: Interpolation Versus Filtered Backpropagation," *IEEE Transactions Acoustics, Speech and Signal Processing*, Vol. 31, No. 5, pp. 1262–1275.
- Santamarina, J. C. and Cesare, M., 1992, "Tomographic Inversion In Vertically Heterogeneous, Anisotropic Media," University of Waterloo, Waterloo, Ontario, Canada.
- Tallin, A. G. and Santamarina, J. C., 1990, "Geotomography in Site Investigations: Simulation Study," *ASTM Geotechnical Testing Journal*, Vol. 13, No. 2.
- Wielandt, E., 1987, "On the Validity of Ray Approximation for Interpreting Delay Times," *Seismic Tomography*, G. D. Nolet, Ed., Reidel Publishing Co., Boston, pp. 85–98.